In Situ Raman Spectroscopy of SiO_2-Supported Transition Metal Oxide Catalysts: An Isotopic $^{18}O-^{16}O$ Exchange Study

Edward L. Lee and Israel E. Wachs*

Operando Molecular Spectroscopy and Catalysis Laboratory, Chemical Engineering Department, 111 Research Drive, Iacocca Hall, Lehigh University, Bethlehem, Pennsylvania 18015

Received: August 12, 2007; In Final Form: January 30, 2008

The molecular structures of dehydrated group 5−7 transition metal oxides (V_2O_5, Nb_2O_5, CrO_3, MoO_3, WO_3, Re_2O_7) supported on SiO_2 were investigated with time-resolved $^{18}O-^{16}O$ exchange in situ Raman spectroscopy measurements. The supported group 5−7 dehydrated surface transition metal oxides were exclusively present as isolated species on SiO_2 because of the absence of bridging M−O−M vibrations. The SiO_2-supported group 5 (VOx and NbOx) surface metal oxides exhibit band splitting into two Raman vibrations (M═^{16}O and M═^{18}O), which is consistent with monoxo surface O═M(−O−Si)$_3$ species. The SiO_2-supported group 6 (CrOx, MoOx, and WOx) surface metal oxides consist of both monoxo O═M(−O−Si)$_4$ and dioxo (O═)$_2$M(−O−Si)$_2$ structures. The dioxo surface species give rise to triplet band splitting corresponding to M(═^{16}O)$_2$, M(═^{18}O)$_2$, and ^{18}O═M═^{16}O. Identification of the intermediate surface ^{18}O═M═^{16}O structure was guided by recent DFT calculations. The SiO_2-supported group 7 (ReOx) metal oxide system exclusively contains trioxo surface (O═)$_3$Re−O−Si species that give rise to quadruplet band splitting (Re(═^{16}O)$_3$, ^{18}O═Re(═^{16}O)$_2$, (^{18}O═)$_2$Re═^{16}O, and (^{18}O═)$_3$Re) during isotopic oxygen exchange. Excellent prediction was also achieved for the isotopic shifts for the completely ^{18}O-exchanged surface metal oxide structures with a simple diatomic oscillator model. The isotopic exchange studies reveal, *for the first time*, the exact number of Raman bands for surface monoxo, dioxo, and trioxo metal oxide structures, their positions, and their band splitting characteristics during isotopic $^{18}O-^{16}O$ exchange.

1. Introduction

Supported metal oxide catalysts consist of a two-dimensional surface metal oxide layer that is 100% dispersed on the support below monolayer coverage or the maximum dispersion limit.[1−3] Such surface metal oxide species terminate with either M−O$^-$, M−OH, M−O−M, or M═O functionalities under dehydrated conditions.[4−9] A major issue surrounding the molecular structures of the supported metal oxide catalysts is the number of terminal M═O bonds (monoxo, dioxo, or trioxo). This issue has usually been addressed with IR and Raman isotopic $^{18}O_2-^{16}O_2$ exchange studies. For example, based on vibrational theory, monoxo species are expected to exhibit two Raman-active vibrational modes (M═^{16}O and M═^{18}O), dioxo species are projected to give rise to three Raman-active vibrational modes (^{16}O═M═^{16}O, ^{18}O═M═^{16}O, and ^{18}O═M═^{18}O), and trioxo species are expected to exhibit four Raman-active vibrational modes (M(═^{16}O)$_3$, ^{18}O═M(═^{16}O)$_2$, (^{18}O═)$_2$M═^{16}O, and M(═^{18}O)$_3$).[10−14] All the reported isotopic oxygen exchange studies, however, have only reported two M═O bands associated with M═^{16}O and M═^{18}O vibrations.[10,15−19] It is puzzling why three or four Raman-active vibrational bands have not been detected for surface oxides of chromium, molybdenum, tungsten, and rhenium. Such contradictions between anticipated and actual vibrational observations have resulted in conflicting structural assignments in the literature. Recent theoretical calculations employing density functional theory (DFT) and normal-mode analysis of model supported MoO_3/SiO_2 and CrO_3/SiO_2, respectively, have suggested that the vibrational structure of partially exchanged surface metal oxide species does not behave as simply as previously thought, and the observed shifts are actually based on the total mass of the surface metal oxide complex.[20,21]

In order to resolve the structural issues surrounding isotopic oxygen exchange of supported metal oxide species and compare the experimental findings with recent theoretical predictions, spectroscopic studies at surface ^{18}O:^{16}O ratios of 0:100, ∼50:50, and ∼99:1 and time-resolved in situ Raman spectroscopy $^{18}O-^{16}O$ exchange experiments of supported MO_x/SiO_2 (M = V, Nb, Cr, Mo, W, and Re) catalysts were undertaken. The SiO_2-supported group 5−7 transition metal oxides (V_2O_5/SiO_2, Nb_2O_5/SiO_2, CrO_3/SiO_2, MoO_3/SiO_2, WO_3/SiO_2, and Re_2O_7/SiO_2) were chosen for investigation because of their well-defined structures.[9] The dehydrated group 5 supported vanadium, niobium, and tantalum oxide catalysts solely consist of isolated surface monoxo O═M(−O−Si)$_3$ species, the group 6 dehydrated supported chromium, molybdenum, and tungsten oxide catalysts predominantly consist of isolated surface dioxo (O═)$_2$M(−O−Si)$_2$ structures and to a lesser extent isolated surface O═M(−O−Si)$_4$ species, and the dehydrated group 7 supported rhenium oxide catalysts contain isolated surface trioxo (O═)$_3$M−O−Si species.[22] These relatively less complex supported metal oxide catalysts represent ideal model systems to understand the more complex molecular structures present in non-SiO_2-supported metal oxide catalysts where isolated and polymeric surface metal oxides can coexist. In addition, the ability to access multiple laser excitations (532, 442, and 325 nm) have allowed the detection of additional vibrational bands not previously reported. The new insights generated from this study resolve the confusion

* To whom correspondence should be addressed. Phone: (610) 758-4274. Fax: (610) 758-6555. E-mail: iew0@lehigh.edu.

10.1021/jp076485w CCC: $40.75
Published on Web 04/03/2008

in the literature and allow for the definitive determination of the number of terminal M═O bonds and molecular structures of the supported metal oxide species on SiO_2 under dehydrated conditions.

2. Experimental Methods

2.1. Catalyst Synthesis. Amorphous SiO_2 (Cabot, Cab-O-Sil fumed silica (EH-5), 332 m^2/g) was employed as the silica support and found to be more easily handled by an initial water pretreatment and calcination at 500 °C for 4 h without changing the material properties.[23−25] The completely dispersed SiO_2-supported metal oxide catalysts (V_2O_5/SiO_2, Nb_2O_5/SiO_2, CrO_3/SiO_2, MoO_3/SiO_2, WO_3/SiO_2, and Re_2O_7/SiO_2) were successfully prepared by incipient wetness impregnation.[22] Other impregnation methods and commercial SiO_2 materials were previously tested and determined not to significantly alter the surface MOx species on SiO_2, which is the focus of the current investigation. In this current preparation, the silica support was impregnated with nonaqueous and aqueous solutions of the corresponding precursors (incipient wetness point of ∼1.2 mL/g SiO_2 with a toluene solvent for nonaqueous preparations and corresponding ∼0.9 mL/g SiO_2 for aqueous preparations): vanadium triisopropoxide ($VO[CHO(CH_3)_2]_3$, Alfa Aesar, 97%), niobium ethoxide ($Nb(OC_2H_5)_5$, Alfa Aesar, 99.999%), chromium(III) nitrate ($Cr(NO_3)_3 \cdot 9H_2O$, Alfa Aesar, 98.5%), ammonium heptamolybdate ($(NH_4)_6Mo_7O_{24} \cdot 4H_2O$, Aldrich, 99.98%), ammonium metatungstate ($(NH_4)_6H_2W_{12}O_{40} \cdot xH_2O$, Pfaltz and Bauer, 99.5%), and perrhenic acid ($HReO_4$, Alfa Aesar, 75−80 wt % in H_2O, 99.9%). The metal oxide loading concentration for each system is accordingly listed in the figure and table captions. The silica was initially dried for 2 h at 115 °C for the nonaqueous preparations prior to impregnation inside a glove box (Vacuum Atmospheres, Omni-Lab VAC 101965) under nitrogen environments. After impregnation, the samples were allowed to dry overnight under the nitrogen atmosphere. Calcination of the samples entailed ramping at 1 °C/min to 110 °C and holding for 5 h under flowing N_2 (Airgas, Ultra High Purity) in a programmable furnace (Thermolyne, model 48000), subsequently followed by another 1 °C/min ramp under flowing air (Airgas, Zero grade) to 500 °C (450 °C for the V_2O_5/SiO_2 for the purposes of following previous work) and held for 6 h. The procedure for the aqueous preparations was the same as the nonaqueous preparations, except that the drying and initial calcination steps were performed in ambient air and under flowing air (Airgas, Zero grade), respectively.

2.2. $H_2{}^{18}O$ Isotopic Exchange. Isotopic oxygen exchange was initially compared using gaseous $^{18}O_2$ and $H_2{}^{18}O$ vapor, and similar spectroscopic results were obtained. An advantage of performing the exchange with $H_2{}^{18}O$ was that the process was more rapid and the almost complete oxygen exchange could be easily achieved. Consequently, only isotopic exchange results with $H_2{}^{18}O$ vapor will be reported. The isotopic ^{18}O exchange was accomplished with $H_2{}^{18}O$ (Isotec, Water-^{18}O, normalized 95 atom% ^{18}O, CAS# 14314-42-2) at elevated temperatures in an in situ environmental cell (Linkam TS1500). The $H_2{}^{18}O$ moisture was directly fed into the heated inlet gas line using a 5 mL liquid syringe (Hamilton, model 1005 LTN), delivered and controlled by a syringe pump (Harvard Apparatus PHD 2000 Infusion, Cat# 70-2100). The lines were kept at a constant temperature of 150 °C to vaporize the $H_2{}^{18}O$. The concentration of isotopic water (0.5−3 mol %) in the gas stream (30−50 sccm Ar) resulted in a liquid flow rate of 0.13−1.4 μL/min of $H_2{}^{18}O$. The concentration of isotopic water was varied depending on the rate of isotopic exchange of the catalyst, which was monitored with online in situ Raman spectroscopy.

It was observed that the more reducible supported CrO_3/SiO_2, MoO_3/SiO_2, and Re_2O_7/SiO_2 catalysts darkened during exposure to the isotopic $H_2{}^{18}O$ vapor with argon as the carrier gas. The darkening of the sample color absorbs the Raman light and somewhat limits the Raman signal from the catalyst surface, likely caused by a slight reduction of the catalyst. To resolve this issue, a small concentration of $^{16}O_2$ was introduced together with the $H_2{}^{18}O$ vapor. This procedure lightened the sample color and yielded strong Raman signals by presumably reoxidizing the catalyst surface. The much more efficient oxygen exchange with $H_2{}^{18}O$ than $^{16}O_2$ assured that the surface MOx species on SiO_2 were populated with ^{18}O. Therefore, the expensive and inefficient gaseous $^{18}O_2$ was not necessary and effectively substituted with $^{16}O_2$. The rate of exchange between gaseous $^{18}O_2$ (5% concentration in inert gas) and liquid $H_2{}^{18}O$ (95% concentration) of the surface species was not performed since the results from the large concentration difference would be tenuous at best.

2.3. In Situ Raman Spectroscopy. The Raman spectra of the SiO_2-supported metal oxide catalysts were obtained with a high-resolution, dispersive Raman spectrometer system (Horiba-Jobin Yvon LabRam HR) equipped with three laser excitations (532, 442, and 325 nm), which has been described earlier.[22] The laser power of the visible lasers at 532 (green) and 442 nm (violet) at the catalyst sample were kept at 10 and 28 mW, respectively, and at 7 mW for the UV laser at 325 nm (not visible). The lasers were focused on the samples with a confocal microscope equipped with a 50× long working distance objective (Olympus BX-30-LWD) for the visible lasers and 15× objective (OFR LMU-15X-NUV) for the UV laser. Laser-induced heating of the sample is negligible since the Raman spectra are collected at high temperatures above 450 °C. The LabRam HR spectrometer was optimized for the best spectral resolution with 900 groves/mm grating (Horiba-Jobin Yvon 51093140HR) for the visible lasers and a 2400 grooves/mm grating (Horiba-Jobin Yvon 53011140HR) for the UV laser. The spectral resolution for both gratings is ∼2 cm^{-1}. Calibration of each laser line was independently measured by a Hg lamp for the zero position and linearity of the gratings. Wavenumber calibration of the Raman spectrograph was checked using the silicon line at 520.7 cm^{-1}. The Rayleigh-scattered light was rejected with holographic notch filters (Kaiser Super Notch) with window cutoffs of ∼100 cm^{-1} for the visible (532 nm) laser, ∼450 cm^{-1} for the visible (442 nm) laser, and ∼300 cm^{-1} for the UV (325 nm) laser. The Raman system was equipped with a UV-sensitive liquid N_2-cooled CCD detector (Horiba-Jobin Yvon CCD-3000V).

The catalyst samples consisted of loose powder, between 5 and 10 mg, and were placed in an environmentally controlled high-temperature cell reactor (Linkam TS1500) containing a quartz window and O-ring seals that were cooled by flowing water. The sample temperature was controlled by a temperature programmer (Linkam TMS94). The sample bed temperature was calibrated externally with a secondary thermocouple where the true bed temperature (Y) versus controller output temperature (X) is corrected and linearly follows $Y = 0.88X$. Other temperature calibration corrections and in situ reactor cell capabilities are detailed elsewhere.[22] Typical reactor cell conditions were 450−700 °C, 10−30 °C/min heating and cooling rates, atmospheric pressure, and ∼30 sccm gas flow rates metered by mass flow controllers (Brooks, model 5850E series). Each dehydrated supported MOx/SiO_2 catalytic system was examined with combined in situ visible (532 and 442 nm) and UV (325 nm) Raman spectroscopy. The Raman laser line that

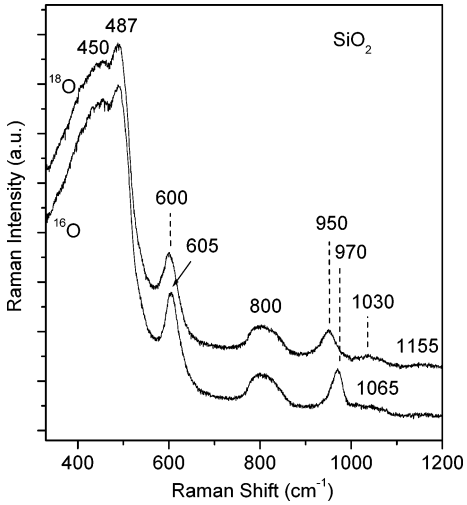

Figure 1. In situ Raman spectra (325 nm) of the dehydrated SiO_2 support at 450 °C under flowing $^{16}O_2$ and after nearly completed exchanged isotopic oxygen with flowing $H_2{}^{18}O$.

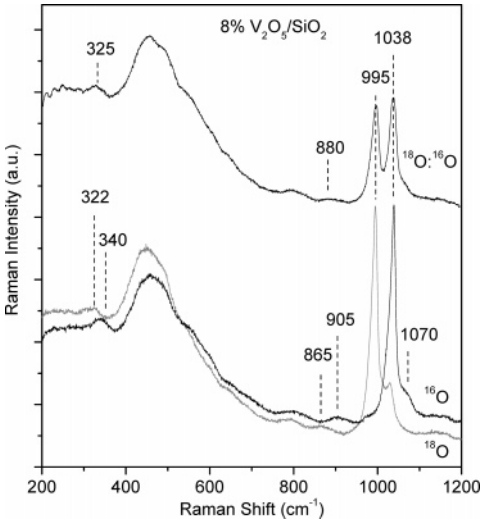

Figure 2. In situ Raman spectra (532 nm) of dehydrated supported 8% V_2O_5/SiO_2 catalyst at 450 °C: ~100% ^{16}O, ~50:50 ratio of ^{18}O:^{16}O, and ~99% ^{18}O.

was best for detecting each surface $M(=O)_x$ species, with emphasis on the $M(=^{18}O)$ $(=^{16}O)$ species, was always employed since no one laser line can provide the best spectra for all materials. The comparison of the effect of different laser excitation energies will be detailed in a subsequent paper. The use of multiple laser excitations avoids sample fluorescence that sometimes plagued earlier Raman measurements and also provides for the potential of resonance enhancement of weak Raman bands that may have been undetected in earlier studies.[26−28]

The protocol for obtaining in situ Raman spectra with isotopic water was as follows. The samples were initially dehydrated in the in situ cell at 500 °C and held for 30 min under flowing 10% O_2/Ar (Airgas, certified, 10.00% O_2/Ar balance). The Raman spectra were collected at 20 s/scan for 20 scans with a 200 μm size hole where only laser angles parallel to the incident beam were acquired from scattering by the catalyst sample. Following the calcination step in oxidizing environments, the in situ cell was purged with Ar (Airgas, UHP) to remove gas-phase molecular O_2. No reduction of the metal oxide species or silica support was observed under the Ar environment. As the gaseous $H_2{}^{18}O$ was introduced at a sample temperature of 400−500 °C, time-resolved Raman spectra were collected to monitor the real-time dynamic changes of the surface metal oxide species during the isotopic oxygen exchange process.

3. Results

3.1. SiO_2 Support. The in situ Raman spectra of the dehydrated SiO_2 support in an $^{16}O_2$ environment and after complete isotopic ^{18}O exchange with $H_2{}^{18}O$ at 450 °C are shown in Figure 1. The unexchanged SiO_2 support gives rise to bands at 970 and 605 cm^{-1} that are assigned to the surface Si−OH stretching mode and D2 defect mode of the three-membered cyclosiloxane ring, respectively.[23,29] After oxygen exchange with isotopic water (labeled as ^{18}O), the Raman band at 970 cm^{-1} shifts to 950 cm^{-1} due conversion of surface Si−^{16}OH to Si−^{18}OH, and the Raman band at 605 cm^{-1} slightly shifts to ~600 cm^{-1}.[29] In addition, weak and broad bands at 1065 and 1200 cm^{-1}, assigned to the transverse-optical (TO) and longitudinal-optical (LO) stretch of the silica network, respectively, shift to ~1030 and 1155 cm^{-1}.[29] Though these bands are weak, the vibrations may become enhanced by different laser lines or when perturbed by metal oxides, as will be shown below. These vibrations, however, are attributed to the silica support. The silica vibrations unaffected by the presence of isotopic water are the silica network bands at ~800 and 410−450 cm^{-1}, assigned to the Si−O−Si symmetrical stretching and network bending modes, respectively.[29−32] Furthermore, the vibrational band at 487 cm^{-1} of the silica D1 defect mode attributed to tetracyclosiloxane rings does not appreciably shift in the presence of oxygen-18.[31,33,34] The vibrations of the SiO_2 support at 487 and 800 cm^{-1} will be employed as internal standards to correct for the coloration effect on the Raman signal intensity because of the varying Raman intensity from color changes by the metal oxide loading during isotopic oxygen exchange as mentioned above. As a control experiment, injection of $H_2{}^{16}O$ vapor under the same experimental conditions was also examined for the $^{16}O_2$-treated SiO_2. No Raman shifts of any silica vibrations were observed upon exposure to $H_2{}^{16}O$ vapor, indicating that during exposure to $H_2{}^{18}O$ only vibrational shifts originating from incorporation of ^{18}O in the catalysts were being observed. The complete time-resolved Raman spectra during the isotopic oxygen exchange process are presented for selected systems. Similar $H_2{}^{16}O$ exposure experiments with the supported MOx/SiO_2 catalysts also demonstrated that exposure to moisture at these elevated temperatures does not affect any of the Raman band positions in the spectra.

3.2. Supported V_2O_5/SiO_2. The surface vanadium oxide species present on the supported V_2O_5/SiO_2 catalyst under dehydrated conditions have been shown to consist of isolated surface $O{=}V(-O-Si)_3$ species and give rise to Raman bands at 1038, 905, and 340 cm^{-1}, shown in Figure 2 and labeled ^{16}O. These Raman bands have been assigned to the terminal $\nu_s(V{=}O)$ stretch, bridging V−O−Si stretch, and δ(O−V−O) bending modes, respectively.[16,22,24,35−41] The sharp band at 1038 cm^{-1} represents the narrow distribution of the surface V=O species, which allows for clear distinction of isotopic surface metal oxide moieties. After nearly complete ^{18}O isotopic exchange, labeled as ^{18}O in Figure 2, the major surface $\nu_s(V{=}O)$ band shifts from 1038 to 995 cm^{-1}, the bridging V−O−Si support vibration shifts from 905 to 865 cm^{-1}, and the bending O−V−O mode shifts from 340 to 322 cm^{-1}. There also appears to be a shift of the band in the 500−600 cm^{-1} region, but the weak vibrations in this range are indistinguishable from that of the silica background. The SiO_2 TO mode, initially present at 1070 cm^{-1}, appears to shift to ~1040 cm^{-1}, but is not clearly

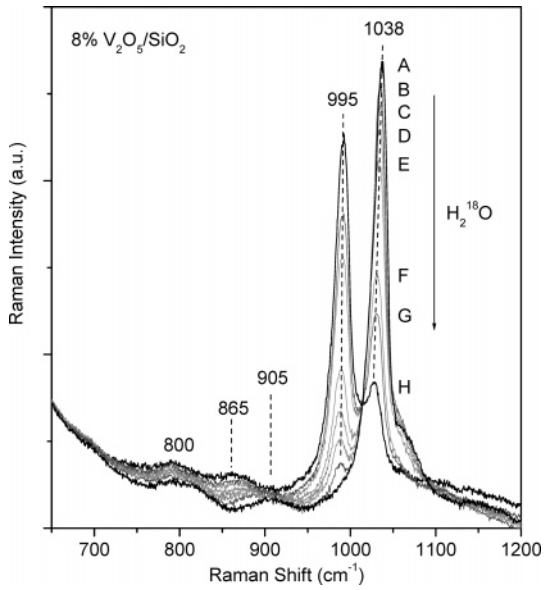

Figure 3. Time-resolved in situ Raman spectra (532 nm) of dehydrated supported 8% V_2O_5/SiO_2 catalyst at 450 °C during oxygen-18 exchange after approximately (A) 0, (B) 10, (C) 20, (D) 30, (E) 40, (F) 70, (G) 90, and (H) 130 min.

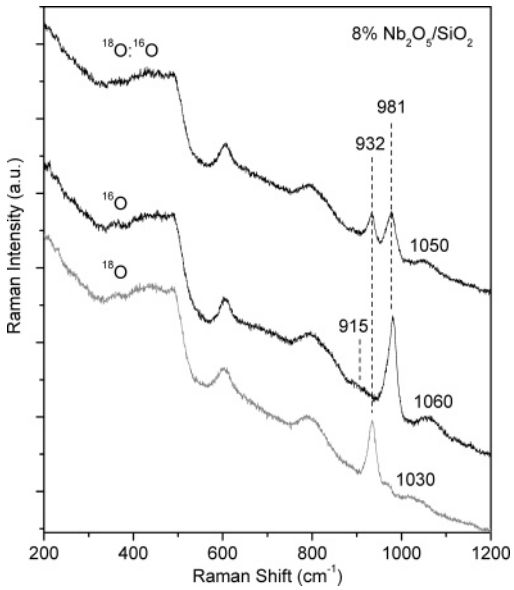

Figure 4. In situ Raman spectra (532 nm) of dehydrated supported 8% Nb_2O_5/SiO_2 catalyst at 600 °C: ~100% ^{16}O, ~50:50 ratio of ^{18}O:^{16}O, and ~100% ^{18}O.

resolved due to overlap with the remaining unexchanged V═^{16}O. In general, the silica support vibrations do not appear to have undergone significant isotopic oxygen exchange, but its vibrations are rather weak relative to the stronger vibrations of the dehydrated surface VO_4 moieties. At intermediate extent of oxygen exchange, labeled ^{18}O:^{16}O in Figure 2, two major Raman bands appear at 1038 and 995 cm^{-1} from the terminal ν_s(V═^{16}O) and ν_s(V═^{18}O) vibrations. The weaker and broad bridging V−O−Si and bending modes shift from 905 to ~880 cm^{-1} and 340 to ~325 cm^{-1}, respectively, reflecting the intermediate extent of isotopic oxygen exchange. The broad nature of the 880 cm^{-1} band is most likely from the summation of the V−^{16}O−Si and V−^{18}O−Si vibrations. From the time-resolved Raman spectra shown in Figure 3, the Raman band positions of the V═^{16}O and V═^{18}O vibrations remain constant during the isotopic oxygen exchange process.

3.3. Supported Nb_2O_5/SiO_2. The surface niobium oxide species present on the supported Nb_2O_5/SiO_2 catalyst under dehydrated conditions have been shown to consist of isolated surface O═Nb(−O−Si)$_3$ species and give rise to Raman bands at 983 and 915 cm^{-1}, shown in Figure 4 and labeled ^{16}O, and assigned to the terminal ν_s(Nb═O) stretching and bridging Nb−O−Si modes, respectively.[25,42−45] The bending δ(O−Nb−O) mode is too weak to observe against the SiO_2 support vibrations in the ~200−400 cm^{-1} region.[22] After almost complete ^{18}O exchange, labeled as ^{18}O in Figure 4, the in situ Raman spectrum only exhibits the ν_s(Nb═^{18}O) band at 932 cm^{-1} and the expected bridging Nb−O−Si band at ~865 cm^{-1} is too weak to be detected against the silica support vibrations. The TO silica network band shifts from ~1060 to 1030 cm^{-1} and slightly decreases in intensity. No other shifts of the other bulk SiO_2 vibrations at 410−450, ~487, and 800 cm^{-1} are observed during the isotopic oxygen exchange. In addition, the remaining weak band at ~960 cm^{-1} is likely due to unexchanged Si−OH or Nb═O vibrations. At intermediate isotopic exchange, labeled ^{18}O:^{16}O in Figure 4, two major Raman bands are present at 981 and ~932 cm^{-1} that are assigned to the symmetric Nb═^{16}O and corresponding symmetric Nb═^{18}O stretches, respectively. The silica TO network band also appears at ~1050 cm^{-1}, which is an intermediate position relative to its vibrations for the two fully exchanged Raman spectra. The Raman band positions of the Nb═^{16}O and Nb═^{18}O vibrations remain constant during the isotopic oxygen exchange process.

3.4. Supported CrO_3/SiO_2. The surface chromium oxide species on the supported CrO_3/SiO_2 catalyst are present as both dioxo (O═)$_2$Cr(−O−Si)$_2$ and monoxo O═Cr(−O−Si)$_4$ surface species, giving rise to major Raman bands for ν_s(Cr(═O)$_2$) at ~980 cm^{-1} and ν_s(Cr═O) at ~1011 cm^{-1}, respectively, demonstrated with the 442 nm excitation.[22,46,47] The asymmetric Cr(═O)$_2$ stretch is expected to vibrate at ~1010−1015 cm^{-1} but is too weak to be detected against the stronger monoxo ν_s-(Cr═O) band in this region. In a previous study, it was shown that the reduction kinetics of the 980 cm^{-1} species differs from the 1011 cm^{-1}, which demonstrates that these two vibrations are not vibrationally coupled and arise from different surface species.[22] The current isotopic oxygen exchange investigation will primarily focus on the dioxo surface (O═)$_2$Cr(−O−Si)$_2$ species with its major ν_s(Cr(═O)$_2$) vibration at ~980 cm^{-1}. It was found that selective Raman enhancement of this dioxo species occurs with UV excitation at 325 nm, which selectively enhances the dioxo vibrations. Therefore, it simplifies the Raman analysis since the vibrations of only one surface species needs to be considered. In addition, only the totally symmetric bands are enhanced with resonance-enhanced Raman,[48,49] specifically the ν_s(Cr(═O)$_2$) species, and not the nontotally symmetric bands; therefore, the asymmetric stretch vibration is not expected to become enhanced. The Raman spectrum of the ~100% surface dioxo (^{16}O═)$_2$Cr(−^{16}O−Si)$_2$ species is presented in Figure 5, labeled as ^{16}O, and using the 325 nm UV laser excitation gives rise to two major Raman bands at 980 and 396 cm^{-1} due to the ν_s(Cr(═^{16}O)$_2$) and bending δ(^{16}O−Cr−^{16}O) vibrations, respectively, with a very weak monoxo Cr═O shoulder band at ~1011 cm^{-1}. After nearly complete isotopic oxygen exchange, labeled as ^{18}O in Figure 5, the in situ Raman bands for the surface dioxo chromia species shift to lower wavenumbers: ν_s(Cr(═^{18}O)$_2$) at 935 cm^{-1} and δ(^{18}O−Cr^{18}O) at 383 cm^{-1}. A weak monoxo ν_s(Cr═^{18}O) should also occur at ~967 cm^{-1} but is obscured by the remaining unexchanged ν_s(Cr(═^{16}O)$_2$). At intermediate extent of isotopic oxygen exchange, labeled ^{18}O:^{16}O in Figure 5, a distinct band at 942 cm^{-1} is prominent when the surface CrO_4 moieties are composed of a mixture of ^{16}O and ^{18}O that

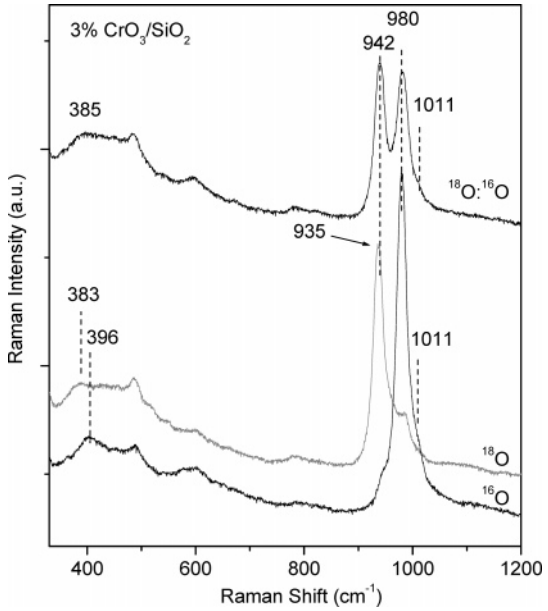

Figure 5. In situ Raman spectra (325 nm) of dehydrated supported 3% CrO_3/SiO_2 catalyst at 500 °C: ~100% ^{16}O, ~50:50 ^{18}O:^{16}O, and ~100% ^{18}O.

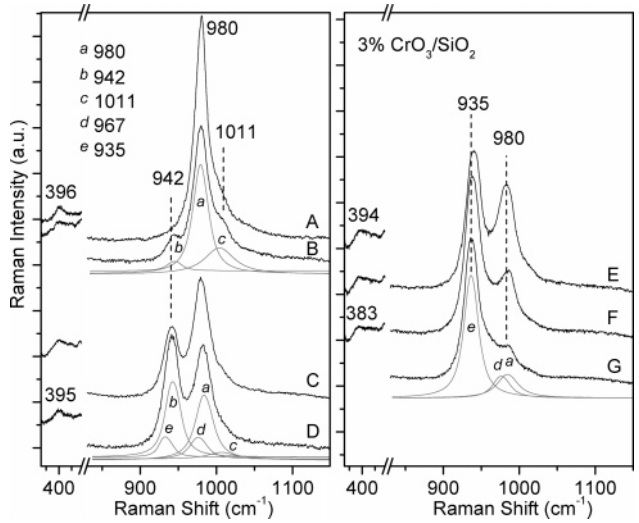

Figure 6. Time-resolved in situ Raman spectra (325 nm) of dehydrated supported 3% CrO_3/SiO_2 catalyst at 500 °C during oxygen-18 exchange after (A) 0, (B) 2, (C) 10, (D) 40, (E) 60, (F) 70, and (G) 90 min. Deconvolution of the spectra are shown in gray and labeled with small letters with the lower case letters *a*−*e* referring to specific band positions indicated in the figure.

further shifts to 935 cm^{-1} for the $\nu_s(Cr(=^{18}O)_2)$ species after complete isotopic oxygen exchange, and the monoxo $\nu_s(Cr=^{16}O)$ band at ~1011 cm^{-1} initially becomes more pronounced as the dioxo $\nu_s(Cr(=^{16}O)_2)$ band at ~980 cm^{-1} more rapidly shifts to lower wavenumbers from the isotopic oxygen exchange. The progression of the isotopic shifts for both of these species is clearly revealed with the time-resolved Raman spectra, shown in Figure 6, where each species is deconvoluted. It is shown that as the $\nu_s(Cr(=^{16}O)_2)$ at 980 cm^{-1} is exchanged, the intermediate species at 942 cm^{-1} arises. Upon further exposure to ^{18}O, the band at 942 cm^{-1} decreases and the band at 935 cm^{-1} of the $\nu_s(Cr(=^{18}O)_2)$ species increases. Concurrently, the $\nu_s(Cr=^{16}O)$ band at ~1011 cm^{-1} shifts to 967 cm^{-1}.

The resonance Raman spectrum of the dehydrated supported CrO_3/SiO_2 catalyst also gives rise to bands in the overtone region (>1000 cm^{-1}) as shown in Figure 7. For the unexchanged

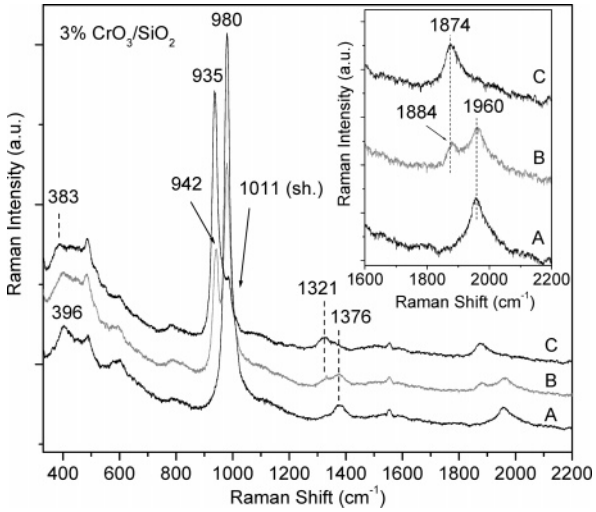

Figure 7. In situ Raman spectra (325 nm) of dehydrated supported 3% CrO_3/SiO_2 at 450 °C including the overtone region: (A) ~100% ^{16}O, (B) intermediate ratio (~1:3) of ^{18}O:^{16}O, and (C) ~100% ^{18}O. (Insert) In situ Raman vibrations in the 1600−2200 cm^{-1} range. The very weak band at ~1550 cm^{-1} is from ambient gas-phase molecular O_2. (Insert) In situ Raman vibrations in the 1600−2200 cm^{-1} range.

sample, Figure 7A, only a single overtone band is present at 1960 cm^{-1} and corresponds to the surface dioxo $2\nu_s(Cr(=^{16}O)_2)$ vibration. The overtone band for the surface monoxo $2\nu_s(Cr=^{16}O)$ vibration should appear at ~2022 cm^{-1} but is not clearly observed because of the selective resonance Raman enhancement of the vibrations of the surface dioxo species. An overtone band at 1376 is also present and assigned to the combination bands of $[\nu_s(Cr(=^{16}O)_2) + \delta(^{16}O-Cr-^{16}O)]$. After nearly complete isotopic exchange, Figure 7C, only a single band is present at 1874 cm^{-1}, assigned to the $2\nu_s(Cr(=^{18}O)_2)$ species. The associated combination band of $[\nu_s(Cr(=^{18}O)_2) + \delta(^{18}O-Cr-^{18}O)]$ occurs at ~1321 cm^{-1}. At intermediate isotopic oxygen exchange, Figure 7B, band splitting occurs with two overtone bands at 1960 and 1884 cm^{-1} from the unexchanged and exchanged $2\nu_s(Cr(=O)_2)$ species, respectively. The combination band of $[\nu_s(Cr(=O)_2) + \delta(O-Cr-O)]$ also exhibits band splitting at 1376 and 1321 cm^{-1}. Further details about the band assignments from the dioxo structure of the intermediate state are found in the discussion section.

3.5. Supported MoO_3/SiO_2. The surface molybdenum oxide species on the supported MoO_3/SiO_2 catalyst are present as both dioxo $(O=)_2Mo(-O-Si)_2$ and monoxo $O=Mo(-O-Si)_4$ surface species, giving rise to Raman bands for $\nu_s(Mo(=O)_2)$ at ~976−988 cm^{-1} and $\nu_s(Mo=O)$ at 1020 cm^{-1}.[4,14,17,22,50−53] The corresponding asymmetric $\nu_{as}(Mo(=O)_2)$ vibration appears as a shoulder at ~965−975 cm^{-1} and the bending $\delta(O-Mo-O)$ mode at ~364 cm^{-1}.[20,22] The Raman spectrum of unexchanged supported 8% MoO_3/SiO_2 is shown in Figure 8 and labeled ^{16}O. The surface dioxo $\nu_s(Mo(=^{16}O)_2)$, $\nu_{as}(Mo(=^{16}O)_2)$, and $\delta(^{16}O-Mo-^{16}O)$ bands appear at 988, 970, and 364 cm^{-1}, respectively. The Raman band of the surface monoxo $\nu_s(Mo=^{16}O)$ species at 1020 cm^{-1} is not present in Figure 8 because of resonance enhancement of the vibrations of the surface dioxo species. In addition, there is a weak shoulder at 932 cm^{-1}, likely arising from the bridging Mo−O−Si bond vibration. After almost complete isotopic oxygen exchange, labeled ^{18}O in Figure 8, the Raman bands for the surface dioxo molybdena species shift to lower wavenumbers: $\nu_s(Mo(=^{18}O)_2)$ at 938 cm^{-1}, $\nu_{as}(Mo(=^{18}O)_2)$ at 920 cm^{-1}, and $\delta(^{18}O-Mo-^{18}O)$ at 352 cm^{-1}. At intermediate extent of isotopic oxygen exchange, labeled ^{18}O:^{16}O in Figure 8, band splitting occurs with the

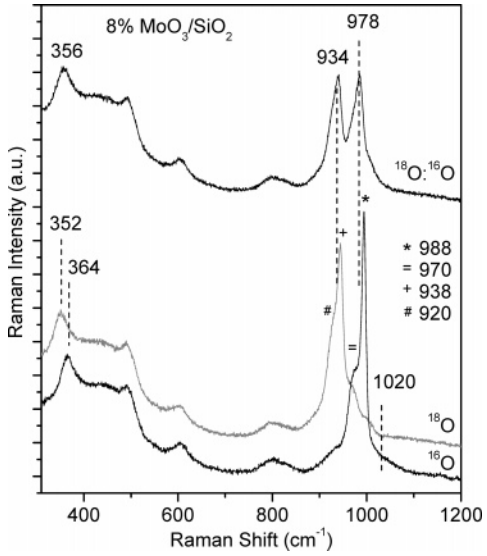

Figure 8. In situ Raman spectra (325 nm) of dehydrated supported 8% MoO_3/SiO_2 at 450 °C: ~100% ^{16}O, ~50:50 ratio of ^{18}O:^{16}O, and ~100% ^{18}O.

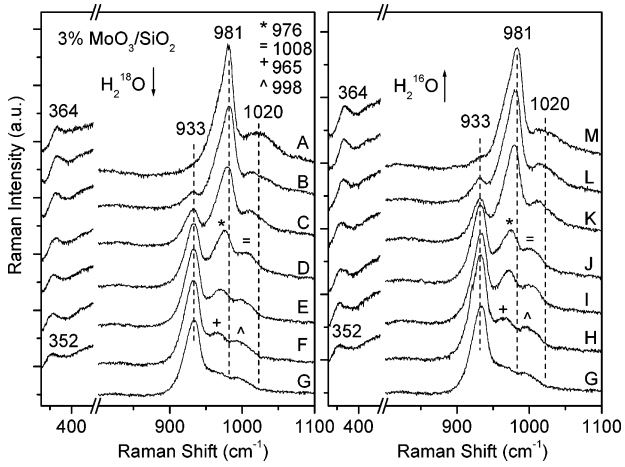

Figure 9. Time-resolved in situ Raman spectra (325 nm) of dehydrated 3% MoO_3/SiO_2 at 500 °C during exposure to $H_2{}^{18}O$ after (A) 0, (B) 5, (C) 20, (D) 30, (E) 40, (F) 70, and (G) 150 min and switching to $H_2{}^{16}O$ after (H) 5, (I) 60, (J) 70, (K) 80, (L) 100, and (M) 110 min of exposure.

$\nu_s(Mo(=^{16}O)_2)$ vibration occurring at 978 cm^{-1} and the $\nu_s(Mo(=^{18}O)_2)$ band at 934 cm^{-1}. The corresponding weak bending $\delta(O-Mo-O)$ mode broadens and is found at 356 cm^{-1}, which is intermediate between that of the ^{16}O- and ^{18}O-containing surface MoO_4 moieties. Note that the $\nu_s(Mo(=O)_2)$ vibration shifts from 988 cm^{-1}, when the surface MoO_4 moieties contain ~100% ^{16}O, to 978 cm^{-1}, when the surface MoO_4 moieties are composed of a mixture of ^{16}O and ^{18}O. The presence of Raman bands that are slightly shifted from those for the complete ^{16}O- or ^{18}O-containing surface MoO_4 moieties are also observed during the time-resolved Raman spectra of the supported 3% MoO_3/SiO_2, as seen in Figure 9. This figure also shows the reversible exchange of the surface ^{18}O to ^{16}O via $H_2{}^{16}O$ (spectra G−M).

In addition to the isotopic oxygen study, the overtone region of the molybdena system was examined with the UV (325 nm) and visible (442 and 532 nm) Raman spectroscopic measurements. Unfortunately, the overtones of the fundamental vibrations were not detected in these Raman spectra.

3.6. Supported WO_3/SiO_2. The dehydrated surface tungsten oxide species on the supported WO_3/SiO_2 catalyst are present as both dioxo $(O=)_2W(-O-Si)_2$ and monoxo $O=W(-O-Si)_4$ surface species, giving rise to Raman bands for $\nu_s(W(=O)_2)$ at ~985 cm^{-1} and $\nu_s(W=O)$ at 1014 cm^{-1}.[22,54] The corresponding asymmetric $\nu_{as}(W(=O)_2)$ vibration appears as a shoulder at ~968 cm^{-1}, which may be overlapping with the Si−OH vibration at ~970 cm^{-1}, and the bending $\delta(O-W-O)$ mode is at ~346 cm^{-1}.[22,52] The in situ Raman spectra of the dehydrated supported WO_3/SiO_2 catalyst with ~100% ^{16}O and ~100% ^{18}O are presented in Figure 10 (labeled ^{16}O and ^{18}O, respectively). The intermediate isotopic oxygen exchange studies encountered sample fluorescence that prevented collection of time-resolved Raman spectra for the supported 6% WO_3/SiO_2 catalyst. After almost complete isotopic oxygen exchange, the dioxo $\nu_s(W(=O)_2)$ band shifts from 985 to 935 cm^{-1} and the monoxo $\nu_s(W=O)$ vibration shifts from 1014 to 963 cm^{-1}. In addition, the surface $\delta(O-W-O)$ mode shifts from 346 to ~330 cm^{-1}, and the $\nu_{as}(W(=O)_2)$ shoulder band at 968 cm^{-1} shifts to ~920 cm^{-1}. The shift of the shoulder band from 968 to 920 cm^{-1} demonstrates that the 968 cm^{-1} band is mostly composed of contribution from the $\nu_{as}(W(=O)_2)$ vibration since $Si-^{18}OH$ only shifts to ~950 cm^{-1} (see Figure 1). The isotopic oxygen shift of the Raman bands in the ~900−1000 and ~300−400 cm^{-1} region confirms that they originate from the surface WOx species since isotopic shifts are not observed for the SiO_2 support vibrations.

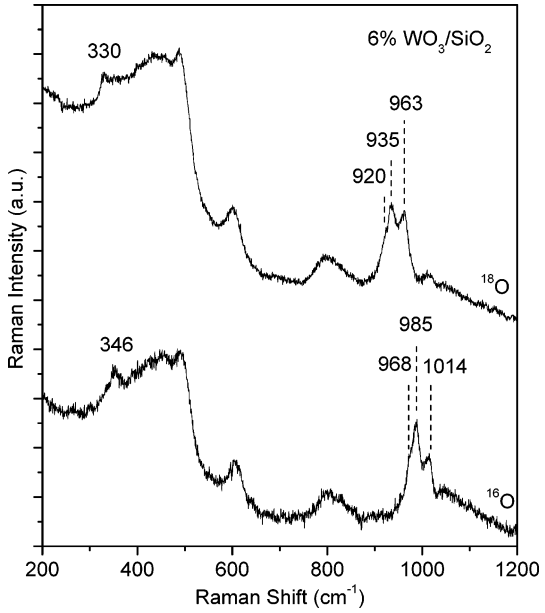

Figure 10. In situ Raman spectra (532 nm) of dehydrated supported 6% WO_3/SiO_2 at 600 °C: ~100% ^{16}O and ~100% ^{18}O.

3.7. Supported Re_2O_7/SiO_2. The dehydrated surface rhenium oxide species on the supported Re_2O_7/SiO_2 catalyst are present as isolated trioxo $(O=)_3Re-O-Si$ species, giving rise to Raman bands for $\nu_s(Re(=O)_3)$ at 1010 cm^{-1}, $\nu_{as}(Re(=O)_3)$ at 977 cm^{-1}, and bending $\delta(O-Re-O)$ at 343 cm^{-1}.[22,55,56] The Raman spectrum of the supported 5% Re_2O_7/SiO_2 catalyst under a $^{16}O_2$/Ar environment is shown in Figure 11A. The vibrations of bridging Re−O−Re bonds at 456 (ν_s) and 185 (δ) cm^{-1} are absent and consistent with the isolated nature of the surface rhenia species on SiO_2. Furthermore, the intensity of the Si−OH vibration at 970 cm^{-1} has been shown with D_2O exchange to only give a small contribution relative to the strong Raman bands of the surface rhenia species on silica.[22] Complete isotopic oxygen exchange of the surface rhenia species under the $H_2{}^{18}O$ vapor environment was not achievable because moisture facilitated the volatilization of the surface rhenia from the SiO_2 support. As a consequence, only time-resolved Raman spectra

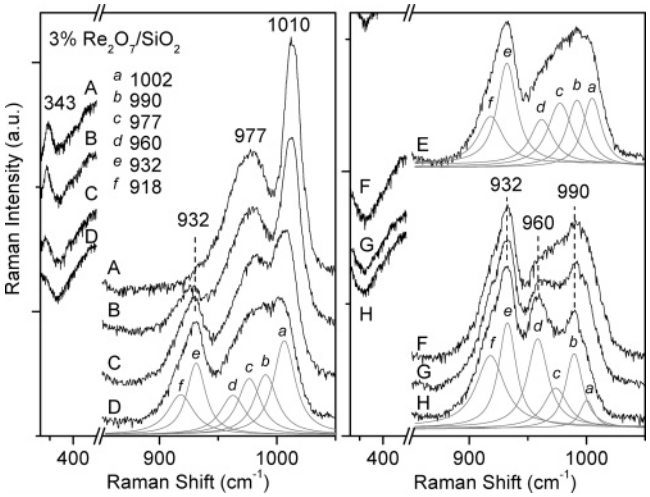

Figure 11. Time-resolved in situ Raman spectra (325 nm) of dehydrated supported 5% Re_2O_7/SiO_2 at 300 °C (A) dehydrated in $^{16}O_2$/Ar and after exposure to $H_2{}^{18}O$ vapor for (B) 5, (C) 25, (D) 34, (E) 51, (F) 60, (G) 76, and (H) 123 min. Deconvolution of the spectra are shown in gray and labeled with small letters with the lower case letters *a*−*f* referring to specific band positions indicated in the figure.

of the early stages of the isotopic oxygen exchange process were collected and are presented in Figure 11.

Upon immediate exposure to isotopic $H_2{}^{18}O$, the $\nu_s(Re(=O)_3)$ band of the surface rhenia species at 1010 cm^{-1} rapidly decreases and shifts to lower wavenumbers because of the incorporation of ^{18}O into the surface ReO_4 moieties (see Figure 11B and C). Concurrently, a new $\nu_{as}(Re(=^{18}O)_3$ band appears at ~932 cm^{-1} at the expense of the initial $\nu_{as}(Re(=^{16}O)_3)$ band at 977 cm^{-1}. The associated bending $\delta(^{16}O-Re-^{16}O)$ mode shifts from 343 to ~335 cm^{-1} as a consequence of the incorporation of the ^{18}O into surface rhenia structure. Upon continued exposure to isotopic $H_2{}^{18}O$, the Raman spectra become more complex due to the presence of multiple band splitting: vibrations at ~1002, 990, ~977, ~960, and 932 cm^{-1} are evident with a small shoulder at ~918 cm^{-1} (see Figure 11D and E). From the spectral deconvolution, shown in gray, the bands can be compared and assigned by band position and intensity. The ~1002 and 990 cm^{-1} bands are tentatively assigned to a single substituted ^{18}O species, $^{18}O=Re(=^{16}O)_2$, and a double substituted ^{18}O species, $(^{18}O=)_2Re=^{16}O$, respectively, where the 990 cm^{-1} band arises at the expense of 1002 cm^{-1}. After still further exchange (see Figure 11F and G), a new vibration at 960 cm^{-1} becomes distinct, tentatively attributed to the triple substituted ^{18}O species, $(^{18}O=)_3Re$, following the decrease of the 977 cm^{-1} band of the $\nu_{as}(Re(=^{18}O)_3$ mode to 932 and 918 cm^{-1}. The ~1002 cm^{-1} band nearly diminishes to a shoulder, giving rise to more intense vibrations at 960 and 990 cm^{-1}. The 932 cm^{-1} band and weak shoulder at ~918 cm^{-1} are tentatively assigned to a fully exchanged $\nu_{as}(Re(=^{18}O)_3)$ vibration with various degrees of distortion. Only the tail of the bending $\delta(O-Re-O)$ mode remains as this band shifts below the window cutoff of the UV notch filter at ~330 cm^{-1} and as ^{18}O becomes incorporated into the surface rhenia structure. At the maximum attainable isotopic exchange (see Figure 11H), only three distinct bands remain at 990, 960, and 932 cm^{-1}, and the 977 and 1002 cm^{-1} vibrations are not present. It is anticipated that if complete isotopic oxygen exchange were achieved, the 990 cm^{-1} band would completely disappear and be replaced with the triply substituted $(^{18}O=)_3$-Re band at 960 cm^{-1}. Further exposure to the $H_2{}^{18}O$ vapor, however, resulted in volatilization of the surface rhenia species as evidenced by blue/purple deposits on the quartz window of the environmental cell and loss of the rhenia Raman signal. An attempt was also made, not shown for brevity, by first reducing the surface ReOx species under hydrogen environments[22] and reoxidizing with either $H_2{}^{18}O$ or $^{18}O_2$, but volatilization still persisted. Nevertheless, detection of four surface rhenia isotopic vibrations $(Re(=^{16}O)_3$ at 1010 cm^{-1}, $Re(=^{18}O)(=^{16}O)_2$ at ~1002 cm^{-1}, $Re(=^{18}O)_2(=^{16}O)$ at 990 cm^{-1}, and $Re(=^{18}O)_3$ at 960 cm^{-1}) is consistent with the trioxo structure of the dehydrated surface ReO_4 moieties on SiO_2.

3.8. Summary of Isotopic Oxygen Exchange Studies for Supported MOx/SiO_2. A summary of the Raman band positions and surface structural assignments of the dehydrated surface metal oxide on SiO_2 containing ^{18}O and ^{16}O is presented in Table 1. Some of the critical issues surrounding each of the SiO_2-supported metal oxide systems are elaborated upon further in the following discussion.

4. Discussion

4.1. Isotopic $H_2{}^{18}O$ Exchange Reaction Mechanism. Oxygen-18 exchange studies via injection of $H_2{}^{18}O$ vapor was found to readily react with both the terminal M=O and bridging M−O−Si surface bonds. It was shown in Figures 2 and 3 for the V_2O_5/SiO_2 system that in the presence of isotopic oxygen the 1038 cm^{-1} band of the $\nu_s(V=^{16}O)$ shifts to 995 cm^{-1} corresponding to $\nu_s(V=^{18}O)$, while concurrently, the 905 cm^{-1} band shifts to 865 cm^{-1} of the bridging $\nu_s(V-^{16}O-Si)$ to $\nu_s(V-^{18}O-Si)$ species. Hydrolysis of $H_2{}^{18}O$, surface isotopic oxygen exchange reaction, and dehydration of $H_2{}^{16}O$ of the sample is proposed to follow the schematic shown for dehydrated group 5 metal oxide catalysts supported on SiO_2 (see Figure 12). The intermediate step is the hydrogen transfer of the ^{18}OH group to the metal−oxygen atoms. The group 6 and 7 metal oxide catalysts containing terminal $M(=O)_2$ and $M(=O)_3$ functional groups, respectively, follow the same reaction cycle. In addition, the Si−OH hydroxyl and silica TO network vibrations of the SiO_2 support containing metal oxides simultaneously exchanges with the isotopic oxygen (see Table 1). The weak $Si-^{16}OH$ vibrations of surface hydroxyls at ~970 cm^{-1}, as seen in Figure 1, readily exchange to $Si-^{18}OH$ at ~950 cm^{-1} in the presence of isotopic $H_2{}^{18}O$. A more apparent vibration is the band at ~1060 cm^{-1}, which is Raman enhanced with the Nb_2O_5/SiO_2 system. This vibration is found to broaden and decrease in intensity while shifting to ~1030 cm^{-1} and agrees with the shift from ~1065 to 1025 cm^{-1} of the silica TO network vibration, similarly observed by isotopically labeled virteous silica.[29] No other shift of the bulk SiO_2 vibrations at ~487, 605, and 800 cm^{-1}, however, are observed in the Raman spectra.

4.2. Molecular Structure of Dehydrated Supported $M^{5+}Ox/SiO_2$. *Supported V_2O_5/SiO_2.* Isotopic oxygen exchange of the dehydrated supported V_2O_5/SiO_2 catalyst results in splitting of the surface V=O band to 1038 and 995 cm^{-1} assigned to $\nu_s(V=^{16}O)$ and $\nu_s(V=^{18}O)$, respectively. The shift from 1038 to 995 cm^{-1} closely matches the theoretical $V=^{18}O$ vibration at 993 cm^{-1} of a simple diatomic oscillator model (see Table 2). The V=O doublet is also consistent with the two bands expected for a surface monoxo metal oxide structure as explained in the Introduction.[11,12,14] The absence of a third intermediate Raman band at ~1015 cm^{-1} from a dioxo $^{16}O=V=^{18}O$ vibration further supports the monoxo V=O structural assignment. Furthermore, only one V=O band at ~2035 cm^{-1} is observed in the overtone region consistent with the dehydrated monoxo surface $O=V(-O-Si)_3$ structure.[35]

Earlier isotopic oxygen studies of V_2O_5/SiO_2 by reduction−reoxidation cycles of gaseous $^{18}O_2$ were not definitive since the

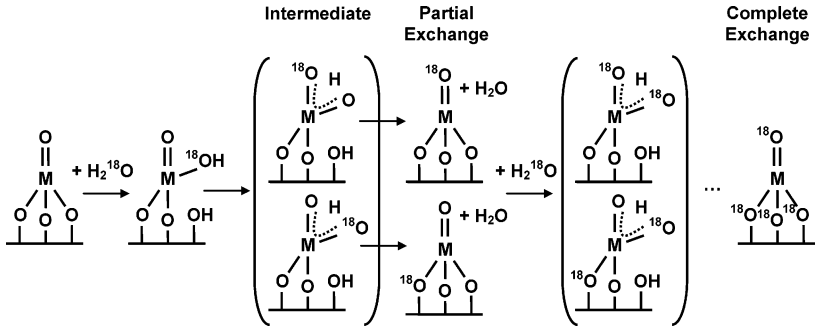

Figure 12. Proposed schematic of isotopic oxygen exchange reaction mechanism with $H_2{}^{18}O$ vapor for an initial and final dehydrated supported group 5 metal oxide catalyst.

TABLE 1: Raman Band Positions (cm^{-1}) of Dehydrated Surface Metal Oxide Species on SiO_2 Containing ^{18}O and ^{16}O with Their Assignments

assignments	SiO_2	V_2O_5/SiO_2	Nb_2O_5/SiO_2	CrO_3/SiO_2	MoO_3/SiO_2	WO_3/SiO_2	Re_2O_7/SiO_2
$\nu_s(Si-{}^{16}OH)$	970 (m)						
$\nu_s(Si-{}^{18}OH)$	950 (m)						
$Si^{16}O_2$ network	1065 (w)	1070 (w)	1060 (w)				
$Si^{18}O_2$ network	1030 (w)	1040[a] (w)	1030 (w)				
$\nu_s(M{=}{}^{16}O)$		1038 (s)	981 (s)	1011 (m)	1020 (m)	1014 (m)	
$\nu_s(M{=}{}^{18}O)$		995 (s)	932 (s)	967[a] (w)	970[a] (m)	963 (m)	
$\nu_s(M(=\,{}^{16}O)_2)$				980 (s)	988 (s)	985 (s)	
$\nu_s(M(=\,{}^{18}O)(=\,{}^{16}O)$				942 (m)	978 (s)	975[a] (m)	
$\nu_s(M(=\,{}^{18}O)_2)$				935 (s)	938 (s)	935 (s)	
$\nu_{as}(M(=\,{}^{16}O)_2)$					970 (m)	968 (w)	
$\nu_{as}(M(=\,{}^{18}O)_2)$					920 (m)	920 (w)	
$\nu_s(M(=\,{}^{16}O)_3)$							1010 (s)
$\nu_s(M(=\,{}^{18}O)(=\,{}^{16}O)_2$							~1002 (m)
$\nu_s(M(=\,{}^{18}O)_2(=\,{}^{16}O)$							990 (m)
$\nu_s(M(=\,{}^{18}O)_3)$							960 (m)
$\nu_{as}(M(=\,{}^{16}O)_3)$							977 (m)
$\nu_{as}(M(=\,{}^{18}O)_3)$							918 (m)
							932 (m)
$\nu_s(M-{}^{16}O-Si)$		905 (w)	~915 (vw)				
$\nu_s(M-{}^{18}O-Si)$		865 (w)					
$\delta({}^{16}O-M-{}^{16}O)$		340 (w)	340[a] (vw)	396 (w)	364 (w)	346 (w)	343 (w)
$\delta({}^{18}O-M-{}^{16}O)$		325 (w)	325[a] (vw)	385 (w)	356 (w)	334[a] (w)	338 (w)
$\delta({}^{18}O-M-{}^{18}O)$		322 (w)	322[a] (vw)	383 (w)	352 (w)	330 (w)	328[a] (w)

[a] Estimated value.

TABLE 2: Theoretical Calculations for the Shift of the $M{=}{}^{18}O$ Species by a Simple Diatomic Oscillator Model[12,13]

		M=O bond (cm^{-1})			
catalyst	isotopic ratio	$[M{=}({}^{16}O)_x]_{expt}$	$[M{=}({}^{18}O)_x]_{expt}$	$[M{=}({}^{18}O)_x]_{th}$	$\Delta({}^{18}O)_{th-expt}$
8% V_2O_5/SiO_2	1.0452	1038	995	993	−2
8% Nb_2O_5/SiO_2	1.0511	981	932	933	1
3% CrO_3/SiO_2	1.0454	980	935	937	2
3% CrO_3/SiO_2	1.0454	1011	967[a]	967	
3% MoO_3/SiO_2	1.0513	981	933	933	0
3% MoO_3/SiO_2	1.0513	1020	980[a]	970	
8% MoO_3/SiO_2	1.0513	988	938	940	2
6% WO_3/SiO_2	1.0554	985	935	933	−2
6% WO_3/SiO_2	1.0554	1014	963	961	−2
5% Re_2O_7/SiO_2	1.0555	1010	960	957	−3

[a] Estimated value.

presence of V_2O_5 crystallites gave rise to a strong band at ~997 cm^{-1} that overlapped with the surface $V{=}{}^{18}O$ vibration at ~995 cm^{-1}.[16] In addition, the earlier isotopic oxygen exchange Raman studies of supported V_2O_5/SiO_2 catalysts did not detect the weak bridging V−O−Si band.[16] A recent Raman study of low-coverage vanadia/silica xerogel catalysts was able to reveal the presence of the V−O−Si stretch band at ~930 cm^{-1}, but this weak vibration was not clearly resolved due to the overlap with Si−OH and the broadening of the bands at higher vanadia loadings.[57] Nevertheless, the ~930 cm^{-1} bridging V−O−Si band shifted to ~900 cm^{-1} after repeated cycles of reduction−reoxidation with gaseous molecular $^{18}O_2$. In the present investigation, the bridging $V-{}^{16}O-Si$ band is found to shift from 905 to 865 cm^{-1} upon formation of the bridging $V-{}^{18}O-Si$ support bond. The clarity of this oxygen-exchanged vibration is particularly useful in identifying the oxygenated species and supports the DFT models and IR evidence. Banares and Wachs also reported that for a supported 2% V_2O_5/SiO_2 catalyst the $V{=}{}^{16}O$ band exists at 1031 cm^{-1} and shifts to 988 cm^{-1} for the corresponding $V{=}{}^{18}O$.[11] The V=O band splitting to two

V═O bands during isotopic oxygen exchange further supports that the surface vanadia species possess a monoxo O═V(−O−Si)$_3$ structure.

Isotopic oxygen exchange with non-SiO_2-supported vanadia catalysts (V_2O_5/TiO_2, V_2O_5/ZrO_2, and V_2O_5/Al_2O_3) also found band splitting with the V═^{16}O band at ∼1025−1035 cm^{-1} and the V═^{18}O band at ∼990−1000 cm^{-1}.[10,11,14,17,19,35,58] In the overtone region, IR exhibits a single overtone band at ∼1965 cm^{-1} for supported V_2O_5/TiO_2[14] and at ∼2030 cm^{-1} for supported V_2O_5/Al_2O_3.[6,35] These isotopic shifts and number of band splittings closely match that for the supported V_2O_5/SiO_2 catalyst.

Supported Nb_2O_5/SiO_2. Isotopic oxygen exchange of the dehydrated supported Nb_2O_5/SiO_2 catalyst parallels that of the supported V_2O_5/SiO_2 system and gives rise to two bands at ∼981 and 932 cm^{-1} that are ascribed to ν_s(Nb═^{16}O) and ν_s(Nb═^{18}O), respectively. Furthermore, these Nb═O bands remain at the same wavenumber location during the isotopic oxygen exchange process. The experimentally observed Nb═^{18}O vibration at 932 cm^{-1} closely matches the theoretically calculated value for a simple diatomic oscillator model at 933 cm^{-1} (see Table 2). The band splitting of the surface Nb═O vibration is consistent with that expected for monoxo surface structures. In addition, the absence of a band at ∼956 cm^{-1} from a surface dioxo ^{18}O═Nb═^{16}O vibration and the lack of an asymmetric surface Nb(═O)$_2$ stretch vibration signify that surface dioxo Nb(═O)$_2$ species are not present. The weak bridging Nb−O−Si support bond is observed at 915 cm^{-1} under molecular $^{16}O_2$ oxidizing conditions,[22] but after isotopic oxygen exchange the small detection "window" between the broad silica vibration at 800 cm^{-1} and the Nb═^{18}O band at 932 cm^{-1} does not allow for a clear distinction of the weak Nb−^{18}O−Si support vibration that is expected at ∼875 cm^{-1}.

The dehydrated surface niobia species present in the supported Nb_2O_5/ZrO_2 catalyst system also undergo band splitting during isotopic oxygen exchange to produce two Nb═O bands at ∼980 and ∼930 cm^{-1} that correspond to the dehydrated monoxo surface O═NbO_3 species present for supported Nb_2O_5/ZrO_2 catalysts.[10] Therefore, the experimental isotopic results suggest that the supported Nb_2O_5/SiO_2 catalyst system also contains monoxo surface O═NbO_3 species.

4.3. Molecular Structure of Dehydrated Supported $M^{6+}Ox/SiO_2$. A brief review of recent computational DFT models for dioxo surface species with isotopic ^{16}O−^{18}O exchange is undertaken to facilitate the spectroscopic assignments and discussion. Bell et al. predicted for supported MoO_3/SiO_2 catalytic systems containing dioxo $O_2Mo(═O)_2$ surface species that the Mo═^{16}O component shifts no more than 5−7 cm^{-1} (995 to ∼988 cm^{-1}) from ν_s(Mo(═^{16}O)$_2$) to ν_s(^{16}O═Mo═^{18}O) and is followed by a large shift of ∼32 cm^{-1} (∼988 to ∼956 cm^{-1}) from the ν_s(^{16}O═Mo═^{18}O) to ν_s(Mo(═^{18}O)$_2$) isotopic species.[20] Furthermore, the Mo═^{18}O component of the isotopic intermediate ^{16}O═Mo═^{18}O species at ∼950 cm^{-1} is probably not detectable since it is calculated to be much less intense than the corresponding Mo═^{16}O component and would also overlap with the ν_s(Mo(═^{18}O)$_2$) vibration. For the corresponding asymmetric stretching mode, DFT calculations predict that the shift of ν_{as}(Mo(═^{16}O)$_2$) to ν_{as}(Mo(═^{18}O)$_2$) is −43 cm^{-1} (from 977 to ∼934 cm^{-1} after complete exchange).[20] It also needs to be noted that the ^{16}O═M═^{18}O symmetric and asymmetric stretching modes, in the fundamental and overtone regions, will not be evident if the dioxo O═M═O bond angle is perpendicular or near 90°.[14,59] Using the DFT calculations as a guide, the experimental results can be assigned accordingly.

Supported CrO_3/SiO_2. Dehydrated CrO_3/SiO_2 possesses ν_s(Cr(═O)$_2$) and ν_{as}(Cr(═O)$_2$) at ∼980 and ∼1010−1015 cm^{-1}, respectively, where in this study selective Raman enhancement of the dioxo species occurs with UV Raman at 325 nm. These vibrations correspond well with DFT-calculated values for a dioxo Cr(═O)$_2$ species, predicted to vibrate at 983/1010 cm^{-1} for the terminal symmetric/asymmetric stretches.[60] The asymmetric stretch mode, however, is expected but not detected with the Raman in the supported CrO_3/SiO_2 spectra suggesting that the O═Cr═O bond angle may be perpendicular or near 90°. The absence of a third, distinct band from the surface ^{18}O═Cr═^{16}O species in the fundamental and overtone regions would also be consistent with the presence of a perpendicular O═Cr═O bond angle.[61] The experimentally observed isotopic shift of −45 cm^{-1} for the ν_s(Cr(═O)$_2$) species in the fundamental region agrees well with the theoretical calculation of a simple diatomic oscillator model at 937 cm^{-1} (see Table 2). This shift is consistent with the reported isotopic shift by Stiegman et al. of −43 cm^{-1} for Cr−silica xerogels from 986 to 943 cm^{-1}.[21]

An alternative scenario that must be considered relates to the detection of an intermediate band at 942 cm^{-1}, assigned to the ν_s(^{16}O═Cr═^{18}O), in the time-resolved isotopic exchange. Following the normal-mode calculations of a (Si−O−)$_2$Cr(═O)$_2$ structural unit, Stiegman et al. predict that for isotopic exchange from ν_s(Cr(═^{16}O)$_2$) to ν_s(^{16}O═Cr═^{18}O) a large shift of −35 cm^{-1} (986 to ∼950 cm^{-1}) will occur followed by a modest −7 cm^{-1} shift (∼950 to 943 cm^{-1}) for ν_s(^{16}O═Cr═^{18}O) to Cr(═^{18}O)$_2$.[21] The experimental isotopic studies presented here exhibit a similar behavior for ν_s(Cr(═O)$_2$) where initially a large shift of −38 cm^{-1} (980 to 942 cm^{-1}) occurs during partial isotopic exchange followed by a small −7 cm^{-1} shift (942 to 935 cm^{-1}) at nearly complete isotopic exchange (see Figure 5). According to the theoretical calculations, the intermediate band at 942 cm^{-1} represents the intermediate ^{18}O═Cr═^{16}O vibration associated with the surface dioxo Cr(═O)$_2$ structure. As for the already weak asymmetric ν_{as}(Cr(═O)$_2$) species, the normal-mode calculations suggest that the ν_{as}(^{16}O═Cr═^{18}O) would not be evident due to overlap with other CrOx vibrations.[21,62] The calculations also predict that a modest change of −9 cm^{-1} (1001 to 992 cm^{-1}) would occur for isotopic exchange from ν_{as}(Cr(═^{16}O)$_2$) to ν_{as}(^{16}O═Cr═^{18}O) and that the weak band at ∼992 cm^{-1} of the ν_{as}(^{16}O═Cr═^{18}O) would inevitably overlap with the intense band at 980 cm^{-1} of the ν_s(Cr(═^{16}O)$_2$) species. Thus, the isotopic oxygen exchange studies with the dehydrated supported CrO_3/SiO_2 catalyst are in agreement with the dehydrated dioxo surface (O═)$_2$Cr(−O−Si)$_2$ structure as the main surface chromia species on SiO_2.

The surface chromia molecular structure in dehydrated support CrO_3/SiO_2 catalysts is different than the dehydrated surface chromia structures present on other oxide supports (Al_2O_3, TiO_2, and ZrO_2).[10,15,63] These non-SiO_2-supported chromia catalysts contain three main CrOx bands that have been assigned to isolated monoxo Cr═O species (1005−1030 cm^{-1}), polymeric monoxo Cr═O (990−1010 cm^{-1}), and bridging Cr−O−Cr vibrations (800−880 cm^{-1}), respectively.[46,64] The absence of bridging Cr−O−Cr bands and the significantly lower wavenumber vibrations found for supported CrO_3/SiO_2 catalysts compared to non-SiO_2 supports demonstrates that the molecular structure of surface dehydrated CrOx species on SiO_2 does not match those of the non-SiO_2 supports. Furthermore, the reduction−reoxidation cycles of oxygen-18 for the supported non-SiO_2 chromia catalysts reveal band splitting to two chromia species at 1030 ν_s(Cr═^{16}O) and 990 cm^{-1} ν_s(Cr═^{18}O), which are the exact band positions expected for a monoxo surface

O═CrO_4 structure.[10,15] Thus, from the experimental isotopic results presented, it is concluded that vibrational and structural differences exist between SiO_2 and non-SiO_2-supported chromia surface species where the dehydrated supported CrOx/SiO_2 system is consistent with isolated surface dioxo $(O═)_2CrO_2$ and isolated surface monoxo O═CrO_4 species.

Supported MoO_3/SiO_2. Dehydrated MoO_3/SiO_2 possesses an intense Raman vibration at 981−988 cm^{-1} (low to high coverage) of the surface $\nu_s(Mo(═O)_2)$ species along with a shoulder at ∼970 cm^{-1} of the corresponding asymmetric stretch and a broad band at 1020 cm^{-1} of the monoxo surface ν_s(Mo═O) species. These vibrations correspond well with recent theoretical DFT studies which predict the vibrational location of dioxo and monoxo molybdena species: 991−995 (ν_s)/967−977 (ν_{as}) cm^{-1} for the dioxo structure and 1014 cm^{-1} (ν_s) for monoxo Mo═O structure.[20] The present study reveals that the dioxo $\nu_s(Mo(═O)_2)$ band shifts from ∼981−988 cm^{-1} to ∼933−935 cm^{-1} after nearly complete isotopic oxygen exchange and also corresponds well to the theoretically calculated Mo═^{18}O vibration of a simple diatomic oscillator model, signifying the good agreement between experimental results and the theoretical model (see Table 2). The shift of approximately −50 cm^{-1} is also consistent with earlier literature observations. Cornac et al. reported with IR that the 990 cm^{-1} band shifts to 940 cm^{-1} during isotopic exchange from Mo^{16}O to Mo^{18}O species, respectively,[50] similarly reported by Seyedmonir and Howe where the 970 cm^{-1} band shifts to 935 cm^{-1} for the Mo═^{16}O to Mo═^{18}O species,[65] and Ohler and Bell[17] observed the shift of the same species from 988 to 938 cm^{-1} by in situ Raman spectroscopy.

Earlier isotopic oxygen exchange studies of dehydrated supported MoOx catalysts reported only a doublet (Mo═^{16}O and Mo═^{18}O) existed under partial isotopic exchange, such as for MoO_3/ZrO_2,[10] resorting to the proposal of a monoxo surface species due to the lack of a distinct third band assigned to the ^{16}O═Mo═^{18}O vibration and the lack of a distinct asymmetric $Mo(═O)_2$ stretch vibration.[10,17] However, these issues can be resolved by the information from the DFT calculations mentioned above for the dehydrated supported MoO_3/SiO_2 catalyst system. The Mo═^{16}O component shifts no more than 5−7 cm^{-1} (995 to ∼988 cm^{-1}) for $\nu_s(Mo(═^{16}O)_2)$ to $\nu_s(^{16}O═Mo═^{18}O)$ and a larger shift of ∼32 cm^{-1} (∼988 to ∼956 cm^{-1}) for the $\nu_s(^{16}O═Mo═^{18}O)$ to $\nu_s(Mo(═^{18}O)_2)$ species.[20] Experimentally, the isotopic results presented in this study exhibit a similar behavior to the DFT calculations where the Mo═^{16}O component initially shifts 5−10 cm^{-1} (981−988 to 976−978 cm^{-1}) followed by a large approximate −40 cm^{-1} shift to ∼933−938 cm^{-1}, which represents the shift from $\nu_s(Mo(═^{16}O)_2)$ to $\nu_s(^{16}O═Mo═^{18}O)$ to $\nu_s(Mo(═^{18}O)_2)$. Therefore, the small initial shift of ∼5−10 cm^{-1} followed by a larger ∼40 cm^{-1} shift indicates the existence of the intermediate ^{16}O═Mo═^{18}O species and allows for the conclusion that the dehydrated surface molybdenum oxide species on silica exist as surface dioxo $(O═)_2MoO_2$ species.

The second issue, the lack of a distinct $\nu_{as}(Mo(═O)_2)$ vibration for dehydrated supported MoO_3/SiO_2 catalysts, is confirmed by isotopic oxygen exchange. DFT calculations predict that the shift of $\nu_{as}(Mo(═^{16}O)_2)$ to $\nu_{as}(Mo(═^{18}O)_2)$ is −43 cm^{-1} (977 to ∼934 cm^{-1}) after complete exchange.[20] It is observed in the experimental isotopic study that the shoulder at 970 cm^{-1} shifts 40−50 cm^{-1} to lower wavenumbers, closely predicted by the DFT calculations for the $\nu_{as}(Mo(═O)_2)$ species. The shoulder shifts to ∼920 cm^{-1} and is consistent as $\nu_{as}(Mo(═^{18}O)_2)$ and not the Si−^{18}OH vibration, which exists at 950 cm^{-1} (see Figure 1).

Supported WO_3/SiO_2. The Raman spectrum after complete isotopic oxygen exchange of dehydrated WO_3/SiO_2 reveals a shift of the two main tungsta species: $\nu_s(W(═O_2))$ shifts from 985 to 935 cm^{-1}, and ν_s(W═O) shifts from 1014 to 963 cm^{-1}. The experimental observations of both WOx vibrations are in excellent agreement with the theoretical calculation for a simple diatomic oscillator model (see Table 2). However, the issue of the $\nu_{as}(W(═O)_2)$ stretch vibration needs to be further examined, which would confirm the presence of a dioxo species. Previous studies have suggested that it is conceivable for the shoulder at 968 cm^{-1} to exist as either an $\nu_{as}(W(═O)_2)$ vibration or the Si−OH hydroxyl group, but reduction of the catalyst under reducing environments to isolate the Si−OH species was ineffective against a stable tungsten oxide overlayer.[22] Therefore, the isotopic oxygen exchange of the dehydrated WO_3/SiO_2 catalyst is particularly critical for the assignment of this band. The band at 968 cm^{-1} shifts from −48 to ∼920 cm^{-1} as a shoulder of the $\nu_s(W(═^{18}O_2))$ at 935 cm^{-1} band and not the Si−^{18}OH vibration, which would occur at 950 cm^{-1}. The large shift, by similarity to the MoO_3/SiO_2 experimental and DFT calculations, validates the assignment of the 968 cm^{-1} band to the $\nu_{as}(W(═O)_2)$ species and not the Si−^{18}OH species, since as mentioned above the ν_s(Si−OH) vibration shifts from 970 to 950 cm^{-1}. The isotopic oxygen shift from 1014 to 963 cm^{-1} for the monoxo ν_s(W═O) vibration on SiO_2 and corresponding bending O−W−O mode shift from 346 to 330 cm^{-1} is in agreement with previously reported isotopic exchange studies for supported WO_3/Al_2O_3 from 1015 to 960 cm^{-1} (ν_s(W═O)) and 350 to 329 cm^{-1} (δ(O−W−O))[66] and for supported WO_3/ZrO_2 from 1005 to 950 cm^{-1} (ν_s(W═O)).[10] Although no isotopic oxygen exchange studies have been reported for supported WO_3/TiO_2, the band position of ν_s(W═O) vibration varies from 1007 to 1016 cm^{-1} as a function of surface tungsten oxide coverage.[3,67−69] The dehydrated supported tungsten oxide species on SiO_2 also give rise to vibrations at 1014 and 346 cm^{-1} that correspond to the vibrations and isotopic oxygen shifts for the non-SiO_2 supports. The predominant surface structure of dehydrated WO_3/SiO_2 catalyst system, however, is the dioxo surface $(O═)_2W(−O−Si)_2$ structure where the 985 cm^{-1} vibration is attributed to the $\nu_s(W(═O)_2)$ and 968 cm^{-1} is assigned to the corresponding $\nu_{as}(W(═O)_2)$.

4.4. Molecular Structure of Dehydrated Supported M^{7+}Ox/SiO_2. *Supported Re_2O_7/SiO_2.* The isotopic oxygen exchange of the dehydrated supported Re_2O_7/SiO_2 system reveals multiple band splittings of the symmetric (four total vibrations) and asymmetric (three total vibrations) $Re(═O)_3$ vibrations corresponding to a trioxo surface Si−O−$Re(═O)_3$ structure. The initial sharp $\nu_s(Re(═^{16}O)_3)$ band at 1010 cm^{-1} sequentially shifts to ∼1002 cm^{-1} for Re(═^{18}O) (═^{16}O)$_2$, 990 cm^{-1} for Re(═^{18}O)$_2$-(═^{16}O), and 960 cm^{-1} for Re(═^{18}O)$_3$. The isotopic shift of the surface $Re(═^{16}O)_3$ vibration at 1010 cm^{-1} to $Re(═^{18}O)_3$ at 960 cm^{-1} corresponds well to the theoretical value of a simple diatomic oscillator model calculated at 957 cm^{-1} (see Table 2). Additionally, the surface $\nu_{as}(Re(═O)_3)$ vibrations shift from ∼977 cm^{-1} to 918 and 932 cm^{-1} for the surface $\nu_{as}(Re(═^{18}O)_3)$ vibrations. The presence of the asymmetric stretch also indicates that more than one terminal Re═O bond is present for the surface rhenia structure on silica. Note that the bridging Re−O−Si band is not detectable with 325 nm excitation.

4.5. Comments on Structural Assignments from Vibrational Spectroscopy. It has been suggested in the early spectroscopy literature, and generally accepted, that the overtone

region should provide additional band splitting not observed in the fundamental region. For instance, polycrystalline bulk V_2O_5 gives rise to three bands[61] at 2025, 1990, and 1975 cm^{-1} of the $2\nu_1$, $\nu_1 + \nu_2$ (combination band), and $2\nu_2$, corresponding to the fundamental[70] observed at $\nu_1 = 1020$ cm^{-1} and $\nu_2 = 985$ cm^{-1}. Extending this finding from bulk oxides to supported metal oxide catalysts for the fundamental ν_s and ν_{as} vibrations suggests the overtone region of a dioxo surface structure should exhibit three vibrations ($2\nu_s$, $2\nu_{as}$, and the $\nu_s + \nu_{as}$) and the overtone region of a trioxo surface structure should give rise to multiple bands (assuming C_{3v} symmetry, $2\nu_s$, $2\nu_{as1}$, $2\nu_{as2}$, $\nu_s + \nu_{as1}$, $\nu_s + \nu_{as2}$, $\nu_{as1} + \nu_{as2}$). From the current Raman study, however, the dehydrated surface dioxo $Cr(=O)_2$ species on silica only give rise to one band in the overtone region. Similarly for the dehydrated surface trioxo $Re(=O)_3$ species on Al_2O_3 that consist of two distinct surface rhenia species, the IR fundamental bands occur at 1015 ($\nu_{s1}(Re(=O)_3)$, 1004 ($\nu_{s2}(Re(=O)_3)$, 980 ($\nu_{as}(Re(=O)_3)$, and 890 cm^{-1} ($\nu_s(Re-O-Al)$), and only two vibrations in the overtone region are present at 1999 and 1972 cm^{-1} from $2\nu_{s1}$ and $2\nu_{s2}$, respectively.[46] If the O=M=O bond angles are at 90°, however, the vibrations will be degenerate and only one ν_s band will appear in the overtone region.[14,59,61] The isotopic oxygen exchange experiments in the fundamental region, however, confirm the surface dioxo $Cr(=O)_2$ and trioxo $Re(=O)_3$ structures with band splitting for CrO_3/SiO_2 at ν_s(980, 942, and 935 cm^{-1}) and for Re_2O_7/SiO_2 at ν_s(1010, 1002, 990, and 960 cm^{-1}). Thus, extreme care should be exercised in making structural assignments strictly based on the number of bands in the overtone region.

5. Conclusions

The structures of the dehydrated surface MOx species present in SiO_2-supported group 5−7 metal oxides have been determined with the aid of time-resolved $^{18}O-^{16}O$ exchange in situ Raman spectroscopy studies. Excellent prediction was achieved with a simple diatomic oscillator model for the completely isotopically exchanged species. The isotopic oxygen exchange study coupled with recent theoretical model studies significantly aided in the determination of the number of terminal M=O bonds in the structures and allowed discrimination between monoxo, dioxo, and trioxo species. The band splitting to two metal oxide components ($M=^{16}O$ and $M=^{18}O$) was observed for the SiO_2-supported group 5 (VOx and NbOx) surface metal oxides and is in exact agreement with the vibrational theory for dehydrated monoxo structures. The SiO_2-supported group 6 (CrOx, MoOx, WOx) metal oxide systems followed vibrational theory for dioxo functionalities for three Raman vibrations; however, detection of the intermediate surface $^{18}O=M=^{16}O$ species was somewhat demanding and guided by recently reported DFT calculations. Both dehydrated surface dioxo $(O=)_2MO_2$ and monoxo $O=MO_4$ structures were found to be present on the silica support. The SiO_2-supported group 7 surface metal oxide, represented by rhenia, was found to follow the expected behavior for a dehydrated surface trioxo functionality: four Raman vibrations representing the various oxygen-exchanged structures of $Re(=^{16}O)_3$, $Re(=^{18}O)(=^{16}O)_2$, $Re(=^{18}O)_2(=^{16}O)$, and $Re(=^{18}O)_3$. These isotopic oxygen exchange studies validate the theoretically allowed number of surface $^{18}O/^{16}O$ permutations for monoxo, dioxo, and trioxo functionalities. The new fundamental insights also resolve conflicting structural assignments in the literature and allow for the definitive determination of the number of terminal M=O bonds and molecular structures of the group 5−7 dehydrated surface metal oxide species present in supported metal oxide species.

Acknowledgment. Funding was provided by the U.S. Department of Energy−Basic Energy Sciences (Grant DE-FG02-93ER14350). We thank Dr. W. Lin of the *Operando* Molecular Spectroscopy and Catalysis Laboratory for his helpful discussions.

References and Notes

(1) Wachs, I. E.; Segawa, K. In *Characterization of Catalytic Materials*; Wachs, I. E., Ed.; Butterworth-Heinemann: Boston, MA, 1992; pp 69−88.
(2) Wachs, I. E. *Catal. Today* **2005**, *100*, 79.
(3) Wachs, I. E. *Catal. Today* **1996**, *27*, 437.
(4) De Boer, M.; Van Dillen, A. J.; Koningsberger, D. C.; Geus, J. W.; Vuurman, M. A.; Wachs, I. E. *Catal. Lett.* **1991**, *11*, 227.
(5) Jehng, J. M.; Wachs, I. E. *Chem. Mater.* **1991**, *3*, 100.
(6) Busca, G.; Ramis, G.; Lorenzelli, V. *J. Mol. Catal.* **1989**, *50*, 231.
(7) Davydov, A. In *Molecular Spectroscopy of Oxide Catalyst Surfaces*; Sheppard, N. T., Ed.; Wiley: Hoboken, NJ, 2003.
(8) Haber, J. Crystallography of Catalyst Types. In *Catalysis: Science and Technology*; Boudart, M.; Anderson, J. R., Eds.; Springer-Verlag: Berlin, 1981; Vol. 2, pp 13−95.
(9) Wachs, I. E. In *Molecular Structures of Surface Metal Oxide Species: Nature of Catalytic Active Sites in Mixed Metal Oxides, in Metal Oxides: Chemistry and Applications*; Fierro, J. L. G., Heinemann, H., Eds.; CRC Taylor & Francis Press: New York, 2005.
(10) Weckhuysen, B. M.; Jehng, J.-M.; Wachs, I. E. *J. Phys. Chem. B* **2000**, *104*, 7382.
(11) Banares, M. A.; Wachs, I. E. *J. Raman Spectrosc.* **2002**, *33*, 359.
(12) Nakamoto, K. *Infrared and Raman Spectra of Inorganic and Coordination Compounds*, 4th ed.; Wiley: New York, 1986.
(13) Banwell, C. N. *Fundametnals of Molecular Spectroscopy*, 3rd ed.; McGraw-Hill; London, 1983.
(14) Busca, G. *J. Raman Spectrosc.* **2002**, *33*, 348.
(15) Weckhuysen, B. M.; Wachs, I. E. *J. Phys. Chem. B* **1997**, *101*, 2793.
(16) Oyama, S. T.; Went, G. T.; Lewis, K. B.; Bell, A. T.; Somorjai, G. A. *J. Phys. Chem.* **1989**, *93*, 6786.
(17) Ohler, N.; Bell, A. T. *J. Phys. Chem. B* **2005**, *109*, 23419.
(18) Jehng, J.-M.; Deo, G.; Weckhuysen, B. M.; Wachs, I. E. *J. Mol. Catal. A* **1996**, *110*, 41.
(19) Wachs, I. E.; Deo, G.; Weckhuysen, B. M.; Andreini, A.; Vuurman, M. A.; de Boer, M.; Amiridis, M. D. *J. Catal.* **1996**, *161*, 211.
(20) Chempath, S.; Zhang, Y.; Bell, A. T. *J. Phys. Chem. C* **2007**, *111*, 1291.
(21) Moisii, C.; Deguns, E. W.; Lita, A.; Callahan, S. D.; van de Burgt, L. J.; Magana, D.; Stiegman, A. E. *Chem. Mater.* **2006**, *18*, 3965.
(22) Lee, E. L.; Wachs, I. E. *J. Phys. Chem. C* **2007**, *111*, 14410.
(23) Gao, X.; Bare, S. R.; Fierro, J. L. G.; Banares, M. A.; Wachs, I. E. *J. Phys. Chem. B* **1998**, *102*, 5653.
(24) Gao, X.; Bare, S. R.; Weckhuysen, B. M.; Wachs, I. E. *J. Phys. Chem. B* **1998**, *102*, 10842.
(25) Jehng, J. M.; Wachs, I. E. *J. Phys. Chem.* **1991**, *95*, 7373.
(26) Tian, H.; Wachs, I. E.; Briand, L. E. *J. Phys. Chem. B* **2005**, *109*, 23491.
(27) Mestl, G.; Srinivasan, T. K. K.; Knözinger, H. *Langmuir* **1995**, *11*, 3795.
(28) Groppo, E.; Damin, A.; Bonino, F.; Zecchina, A.; Bordiga, S.; Lamberti, C. *Chem. Mater.* **2005**, *17*, 2019.
(29) Galeener, F. L.; Mikkelsen, J. C., Jr. *Phys. Rev. B* **1981**, *23*, 5527.
(30) Brinker, C. J.; Kirkpatrick, R. J.; Tallant, D. R.; Bunker, B. C.; Montez, B. *J. Non-Cryst. Solids* **1988**, *99*, 418.
(31) McMillan, P. *Am. Mineral.* **1984**, *69*, 622.
(32) Galeener, F. L.; Geissberger, A. E. *Phys. Rev. B* **1983**, *27*, 6199.
(33) Morrow, B. A.; Mcfarlan, A. J. *J. Non-Cryst. Solids* **1990**, *120*, 61.
(34) Uchino, T.; Tokuda, Y.; Yoko, T. *Phys. Rev. B* **1998**, *58*, 5322.
(35) Resini, C.; Montanari, T.; Busca, G.; Jehng, J. M.; Wachs, I. E. *Catal. Today* **2005**, *99*, 105.
(36) Banares, M. A.; Cardoso, J. H.; Agullo-Rueda, F.; Correa-Bueno, J. M.; Fierro, J. L. G. *Catal. Lett.* **2000**, *64*, 191.
(37) Das, N.; Eckert, H.; Hu, H.; Wachs, I. E.; Walzer, J. F.; Feher, F. J. *J. Phys. Chem.* **1993**, *97*, 8240.
(38) Burcham, L. J.; Deo, G.; Gao, X.; Wachs, I. E. *Top. Catal.* **2000**, *11/12*, 85.
(39) Went, G. T.; Oyama, S. T.; Bell, A. T. *J. Phys. Chem.* **1990**, *94*, 4240.
(40) Deo, G.; Wachs, I. E. *J. Catal.* **1994**, *146*, 323.
(41) Magg, N.; Immaraporn, B.; Giorgi, J. B.; Schroeder, T.; Baumer, M.; Dobler, J.; Wu, Z.; Kondratenko, E.; Cherian, M.; Baerns, M.; Stair, P. C.; Sauer, J.; Freund, H. J. *J. Catal.* **2004**, *226*, 88.

(42) Gao, X.; Wachs, I. E.; Wong, M. S.; Ying, J. Y. *J. Catal*. **2001**, *203*, 18.
(43) Burcham, L. J.; Datka, J.; Wachs, I. E. *J. Phys. Chem. B* **1999**, *103*, 6015.
(44) Maurer, S. M.; Ko, E. I. *J. Catal.* **1992**, *135*, 125.
(45) Huuhtanen, J.; Sanati, M.; Andersson, A.; Andersson, S. L. T. *Appl. Catal. A* **1993**, *97*, 197.
(46) Vuurman, M. A.; Wachs, I. E.; Stufkens, D. J.; Oskam, A. *J. Mol. Catal*. **1993**, *80*, 209.
(47) Weckhuysen, B. M.; Wachs, I. E. *J. Phys. Chem. B* **1996**, *100*, 14437.
(48) Smith, W. E.; Dent, G. *Modern Raman Spectroscopy−A Practical Approach*; John Wiley & Sons, Inc.: New York, 2005.
(49) Long, D. A. *The Raman Effect*; John Wiley & Sons, Inc.: New York, 2002.
(50) Cornac, M.; Janin, A.; Lavalley, J. C. *Polyhedron* **1986**, *5*, 183.
(51) Williams, C. C.; Ekerdt, J. G.; Jehng, J.-M.; Hardcastle, F. D.; Turek, A. M.; Wachs, I. E. *J. Phys. Chem.* **1991**, *95*, 8781.
(52) Hu, H.; Bare, S. R.; Wachs, I. E. *J. Phys. Chem.* **1995**, *99*, 10897.
(53) Banares, M. A.; Hu, H.; Wachs, I. E. *J. Catal.* **1994**, *150*, 407.
(54) Kim, D. S.; Ostomecki, M.; Wachs, I. E.; Kohler, S. D.; Ekerdt, J. G. *Catal. Lett.* **1995**, *33*, 209.
(55) Vuurman, M. A.; Stufkens, D. J.; Oskam, A. *J. Mol. Catal.* **1992**, *76*, 263.
(56) Kim, D. S.; Wachs, I. E. *J. Catal.* **1993**, *141*, 419.
(57) Moisii, C.; Curran, M. D.; van de Burgt, L. J.; Stiegman, A. E. *J. Mater. Chem.* **2005**, *15*, 3519.
(58) Ramis, G.; Cristiani, C.; Forzatti, P.; Busca, G. *J. Catal.* **1990**, *124*, 574.
(59) Lever, A. B. P. *Inorganic Electronic Spectroscopy*; Elsevier: New York, 1968.
(60) Dines, T. J.; Inglis, S. *Phys. Chem. Chem. Phys.* **2003**, *5*, 1320.
(61) Busca, G.; Lavalley, J. C. *Spectrochim. Acta* **1986**, *42A*, 443.
(62) Czernuszewicz, R. S.; Spiro, T. In *Inorganic Electronic Structure and Spectroscopy*, 1st ed.; Solomon, E. I., Lever, A. B. P., Eds.; Wiley: New York, 1999; Vol. 1, p 732.
(63) Hardcastlle, F. D.; Wachs, I. E. *J. Mol. Catal.* **1988**, *46*, 15.
(64) Kim, D. S.; Wachs, I. E. *J. Catal.* **1993**, *142*, 166.
(65) Seyedmonir, S. R.; Howe, R. F. *J. Catal.* **1988**, *110*, 216.
(66) Stencel, J. M.; Makovsky, L. E.; Diehl, J. R.; Sarkus, T. A. *J. Raman Spectrosc.* **1984**, *15*, 282.
(67) Vuurman, M. A.; Wachs, I. E. *J. Phys. Chem.* **1992**, *96*, 5008.
(68) Vuurman, M. A.; Wachs, I. E.; Hirt, A. M. *J. Phys. Chem.* **1991**, *95*, 9928.
(69) Kim, D. S.; Ostromecki, M.; Wachs, I. E. *J. Mol. Catal. A* **1996**, *106*, 93.
(70) Sanchez, C.; Livage, J.; Lucazeau, G. *J. Raman Spectrosc.* **1982**, *12*, 68.